A new experimental method for tensile property study of quartz sandstone under confining pressure

Zaobao Liu, Hongyuan Zhou, Wang Zhang, Shouyi Xie, Jian-Fu Shao

A new experimental method for tensile property study of quartz sandstone under confining pressure

Zaobao Liu[1, 2*], Hongyuan Zhou[1], Wang Zhang[2], Shouyi Xie[2], Jianfu Shao[1, 2*]

[1] Key Laboratory of Ministry of Education on Safe Mining of Deep Metal Mines, College of Resources and Civil Engineering, Northeastern University, Shenyang, 110819, China

[2] University of Lille, CNRS, LaMcube, FRE2016, F-59000 Lille, France

* Corresponding authors, Email: liuzaobao@mail.neu.edu.cn; jian-fu.shao@polytech-lille.fr, Phone: 00-33-320434626; Fax: 00-33-320337153

Author ORCID: Zaobao Liu: 0000-0002-2047-5463; Jianfu Shao: 0000-0002-6632-8207

Abstract: Tensile strength of rocks is an important parameter involved in the design and stability analysis of rock structures. The present paper is devoted to develop a new experimental method to investigate tensile strength, and the effect of confining pressure (P_c) on tensile behavior of rocks in underground rock engineering. A triaxial direct tension (noted as TDT) apparatus was developed based on the conventional triaxial compression (noted as CTC) device with the inspiration of the glue on steel cap type of method. TDT tests were carried out on the Fontainebleau quartz sandstone specimens under four different confining pressures. CTC tests under nine confining pressures were also carried out in order to compare the tension and compression behavior of the tested quartz sandstone. Tensile stress-strain curves were obtained during the CTC and TDT tests. Post-failure specimen analysis was also carried out to identify the failure mode in TDT test. The triaxial tension failed surfaces was sampled and scanned with the optical microscopy to obtain three dimensional images to show the effect of the confining stress on the failed surface roughness. The relationship between tensile and compressive strength and the strength criteria were analyzed with the experimental data. The results show the failure mechanism under TDT loading is different from that under CTC. The inter-grain cement is the dominant factor that contributes to the triaxial tensile strength of the quartz sandstone although the increase of confining pressure can induce a decrease of the triaxial direct tensile strength. It is suggested that the direct tensile strength of rocks should be tested directly for underground structures that confining pressure exists since uniaxial tensile strength can induce overestimate of the triaxial tensile strength.

Keywords: triaxial tensile strength; TDT device, experimental rock mechanics, tensile strength criterion, tensile failure

1 Introduction

Tensile failure is an important issue in the mechanisms of rock blasting, rock borehole breakout, rock roof and floor failure, rock drilling and mineral extraction technology etc., particularly because rocks are very much weaker in tension than in compression. It is then imperative to study tensile failure process of rocks in depth. Among others, tensile strength of rocks is an essential parameter involved in the design and stability analysis of rock structures. In underground rock engineering, rock tensile strength limits the dimension of the roof span of underground openings[1] and the borehole pressure for hydraulic fracturing[2]. Therefore, it is critical to accurately characterize the tensile behavior of rocks for the design and stability analysis of underground rock engineering.

Tensile strength of brittle materials has been widely investigated worldwide since the first introduction of an indirect tensile strength testing method for concrete in 1943 [3, 4] due to its easiness in implementation. Nowadays the method is known as the Brazilian or the indirect tensile strength test and has been developed with many modifications to improve its accuracy in estimation of the tensile strength of brittle rock-like materials. There are four typical loading platen arrangements as suggested by the ISRM, i.e. the flat loading platens, the flat platens with cushion (often wood), the flat loading platens with small diameter rods, or the flat loading platens with curved loading jaws [5]. As concluded in the review, the research on the Brazilian test in the field of rock mechanics became rejuvenated over the past 70 years [6]. The tensile strength in the Brazilian test was concluded (or argued) to be an experimental system property and not a material property [7, 8] since the value of the obtained tensile strength largely depends on the specimen length-to-diameter ratio [9], the rock nature (elastic and brittle), and the loading arrangement.

To improve the uncertainty in the Brazilian indirect tensile strength method, many other methods have been also introduced to determine the tensile strength of rocks. These methods include the indirect testing method [6-8, 10-14], direct testing method [2, 5, 15-26] and correlation-based estimation method [19, 27, 28]. It is further found that it is very difficult to obtain an accurate estimation of tensile strength from other rock properties, such as uniaxial compression strength (UCS). The correlation of tensile strength with other properties could be used only for the preliminary assessment of tensile strength in engineering applications but the actual testing is always recommended since the rock tensile strength is largely scattered due to the rock type, mineralogy, and loading conditions [28].

A major advantage of the indirect testing method is the implementation simplicity that is the main reason of its wide usage in spite of many uncertainties involved in the determination of the tensile strength. On the

other hand, the advantage of the direct method is its accuracy if all the experimental issues can be under control. With the progress in sample fabrication and gluing technologies, the direct method has newly redrawn more and more attention due to the need in large-scale underground rock engineering[20, 21]. The development of the direct testing method involves uniaxial tension test on the dog-bone-shape specimen [23], the dumbbells-shape specimen [2, 25], and/or the cylindrical specimen [20, 29-31]. All the improvements and modifications so far aimed at and have succeeded in determining more precisely the tensile strength of rocks under uniaxial tension state.

However, rocks in underground engineering are under constraints due to the in-situ stress that makes the tension failure of underground rocks far from that in the uniaxial tension test. Therefore, it is required to develop a new experimental method and device that can realize tension failure tests on rock samples under lateral stress to determine more precise the rock tensile strength and to better understand the tensile behavior of rocks under triaxial stress conditions. The present study is devoted to the development of a new TDT (TDT) device and to the study of confining pressure (P_c) effect on the rock tensile strength.

The manuscript is organized into four parts. Section 2 introduces the development of the TDT device with a review on sketch design of uniaxial tension and CTC. Section 3 introduces the tested materials and experimental procedure with the new device to derive expected experimental results. Section 4 presents the results of the TDT tests under four different lateral stresses and the results of CTC (CTC) tests under nine different confining pressures. Section 5 presents a discussion of the strength of the tested Fontainebleau sandstone. Throughout the paper, positive sign is for compressive stress and negative sign is for tensile stress.

2 TDT device

2.1 Recall of direct tension apparatus

Although the TDT device has rarely been reported in the literature, there are many types of direct tension apparatus for uniaxial tensile strength testing. The method of direct tension of rocks, in principle, is similar to that employed in the test of metal materials. However, the principal difficulty in the direct tension test of rocks is the gripping of specimens and the application of a load parallel to the axis of the specimen. Specially prepared specimens are required to get uniform tensile stress distribution and for easy gripping [26]. Although it is difficult to make the gripped specimen, several specimen shapes and methods of attaching specimens to the pulling system have been used by investigators engaged in the determination of tensile strength of rocks.

A grip was proposed to carry out tension test of rocks shown in Fig. 1 (a) [29]. In this test apparatus, a cylindrical specimen is held in place with a Leadite compound cast around each end of the specimen forming a bearing surface. The grips are in direct contact with the Leadite cast and do not touch the specimen. A spherically seated joint in the grip cups is placed close to the end of the specimen and in line with the axis of the specimen. This special design permits self-alignment in the test apparatus. After testing a large number of specimens of marble, limestone, granite, sandstone, etc., it was reported that Leadite compound is not suitable to hold specimens with tensile strength greater than 8.27 MPa. The method is also suffering from gripping and preparation of samples of special shapes.

To overcome these difficulties, a typical method using cylindrical specimens and epoxy based cements (of approximately 20.69-27.58MPa tensile strength) was devised [30]. The specimen is glued to the steel caps as shown in Fig. 1 (b) and loaded with the help of a flexible cable using a simple cantilever arrangement. For gluing, the adhesive EC 1838B/A was used. A narrow lip of 0.008cm high was made on to the cap ends to ensure that cement from the rock-steel interface is not extruded during curing. This method is reliable and gives relatively consistent results. It is satisfactory among the various tests conducted for direct determination of tensile strength of many rocks. The preparation of specimen is also very simple and either cylindrical and square or rectangular specimens can be used in this method [32]. For very strong rocks, it is also difficult to develop sufficient bond strength. The end conditions become similar to those prevailing in the conventional compressive strength test with complete end restraint. However, since most cables are made of twisted strands of steel, they may introduce torque into the test specimen.

The dog-bone shape specimens were also a type of testing for tensile strength of rocks [23]. Besides, another technique was reported with the usage of Aluminum collars [31] designed to approximate the effect of rock fillets (See Fig. 1 (c)). A cylindrical specimen is cemented into chamfered Aluminum collars which are machined to allow a clearance of approximately 80μm between rock and Aluminum. The two are then slotted longitudinally to minimize hoop stress and provide some radial and circumferential strain freedom. In this method however, there is an unavoidable tendency for fracture at the collar also.

The above three types of direct tension apparatus are the basic ones in rock tensile strength testing although later investigator have either improved or modified the design. From the typical types of direct tension apparatus, one can conclude it is important that the specimen be mounted in the tension grips without damaging the specimen surface. Besides, there will be a tendency to cause torsion, bending, and producing abnormal stress concentrations if the centralization is not perfectly controlled.

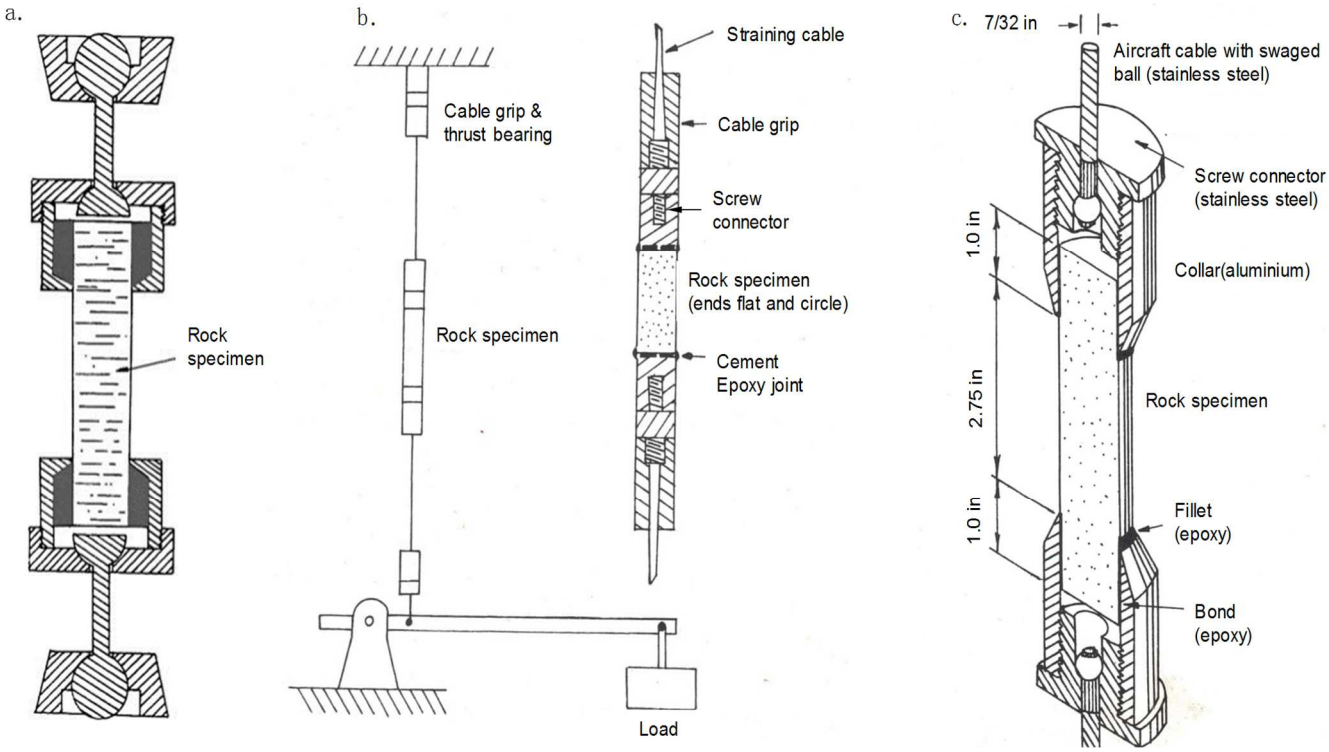

Fig. 1 Typical direct tension testing apparatus for rock tensile strength determination

2.2 Design of TDT apparatus

Inspired by the previous direct testing methods, we developed a TDT apparatus based on our conventional triaxial compressive testing device [33, 34]. The sketch of the TDT apparatus is shown in Fig. 2. The main components of the apparatus are the same as those of our CTC testing device that has been proven to have a good performance in rock triaxial compressive testing [35-39]. The modifications from the CTC apparatus include the tension chamber and the axial pulling components with the accessories as shown in Fig.2. The loading piston is devised to be able to apply either a compressive or a tensile stress in the axial direction of the specimen by controlling the pressures in the two chambers separated by the wing of the piston. Screwing connections are used between the steel components such as the pull rod, the specimen supporting head. Cement connection is used between rock specimen and its supports. Cement is critical important in the sample preparation to adapt the rock property, e.g. dry and clean surface. The centralization of all the pieces is another important point in the tension apparatus. Thanks to the fabrication technology, centralization of steel components nowadays has become easier. The key controlling procedure is thus the centralization of specimen with the steel components.

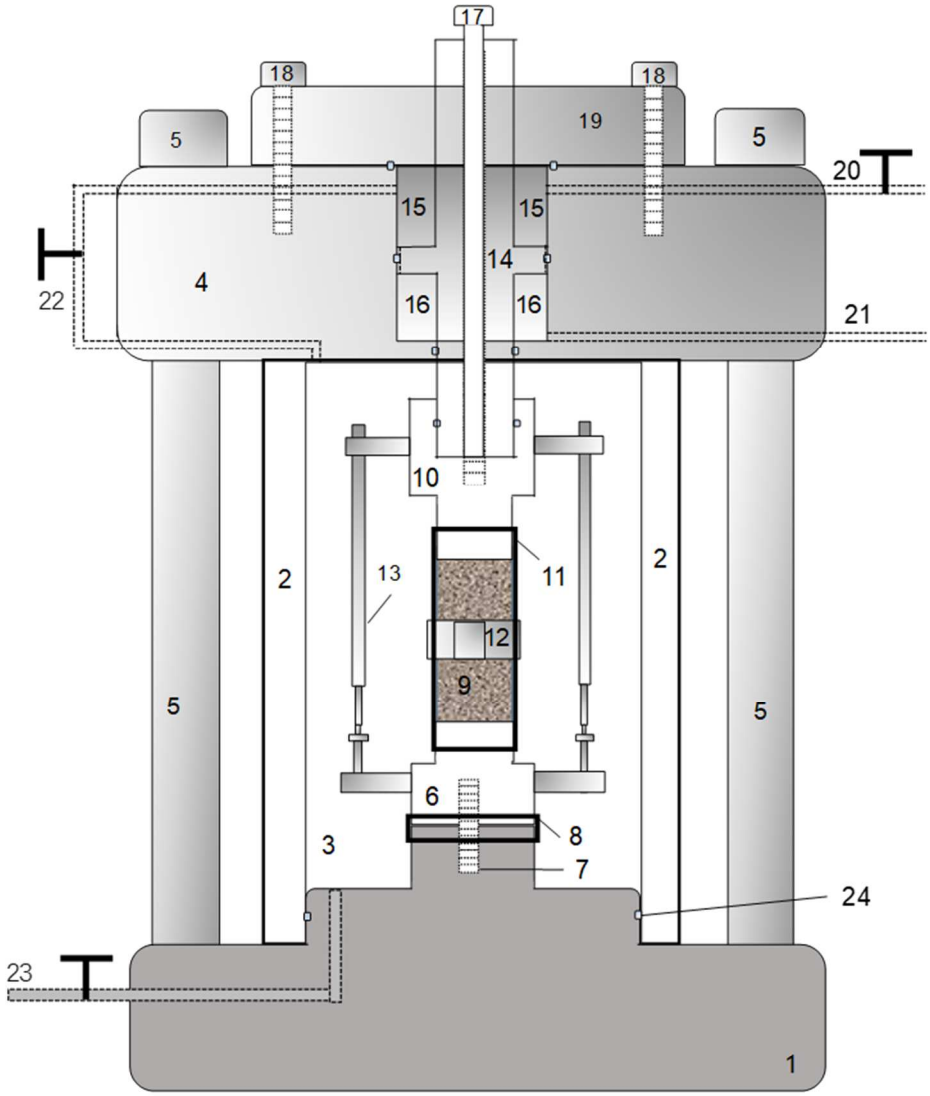

1-device base 2-triaxial cell chamber wall 3-triaxial chamber 4-chamber cap 5-pull rod with screw into 2
6-specimen supporting base 7-connecting screw 8-sealing jacket 9-specimen
10-specimen supporting head for pulling 11-specimen sealing jacket 12-ring for radius strain measurement
13-LVDT for axial strain measurement 14-loading piston 15-autocompensated chamber
16-tension force production chamber 17-pull rod with screw into 10 18-screwing rod
19-sealing cap of chamber 15 20-tube with valve between chamber 15 and the outside
21-tube with valve between chamber 16 and a hydro-servo pump for direct tension loads
22-tube with a valve between chamber 3 and 15
23-tube connecting to a hydro-servo pump for confining pressure loading

Fig. 2 Sketch of TDT apparatus

The cylindrical specimen is cemented onto the surface of the supporting base at one end and to the supporting head for pulling at the other end during sample preparation process. The supporting bases have the same diameter as the tested specimen to minimize stress concentrations at the cemented surface. The cementation is very important during sample preparation. To realize good cementation, the DELO-CA cement (approximate 25MPa tensile strength) was used and a cementing and curing device (shown in Fig. 3) was

devised to better centralize the specimen with the supporting bases during the cement curing (24 hours or more) in the plastic sealing jacket. Prior to testing, the specimen, together with the supporting bases, is screwed into the device base by the connecting screw. The contacting surface at the connecting screw is sealed by the sealing jacket from the confining pressure.

At a given confining pressure, the specimen in the triaxial cell is compressed by an isostatic stress. When pressure is increased in the tension chamber by a hydro-servo pump, the axial compressive stress applied to the specimen is reduced firstly. The axial tensile stress will arise in the specimen if the pressure in the tension chamber is increased to be higher than the confining pressure. Then, the specimen will behave in axial direct tension stress state under the given confining pressure. If no confining pressure is applied, the apparatus can realize the uniaxial tension test.

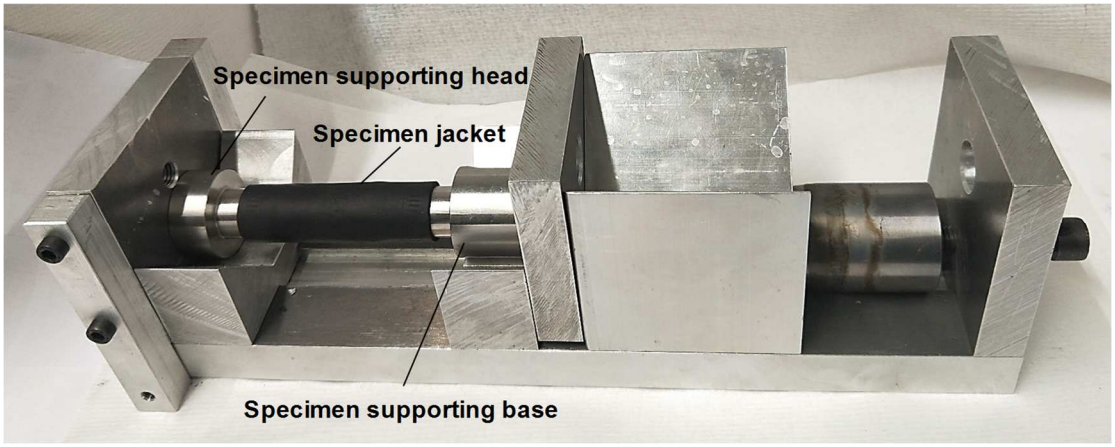

Fig. 3 Specimen cementing and curing device

2.3 Technical details of developed apparatus

In the developed TDT apparatus, we can measure pressure, stress, displacement, and strain by sensors. The confining pressure is applied by the ISCO D260 series pump with the maximal pressure value of 600 bars and precision of 0.1 bars. Pressure injection into the tension force production chamber is done by another Gilson pump that can control the inject flow rate from 0.0005 ml/min to 5 ml/min and has the maximal pressure value of 600 bars with precision of 0.1 bars. The axial displacement is measured by a pair of LVDTs that has a measurement range of 0 to 10 mm with precision of 0.001 mm. The radius change is measured by a circumferential ring that has a measurement range of 1.5 mm and precision of 0.001 mm. The precision of the ring is lower than the LVDT due to technical reasons in component arrangement. As an option, both the axial

and radius strains can be measured by the strain gages, which however requires more time for sample preparation. Thus, we used the LVDTs and circumferential ring to measure the strains during stress loading.

The pressure applied on the specimen is measured by the pressure sensors that have a measurement range of 0 to 200 bars and a precision of 0.01 bars. The stress is calculated from the pressure measured by the pressure sensors. The lateral (radial) stress σ_r is equal to the confining pressure P_c, i.e.

$$\sigma_r = P_c \tag{1}$$

The axial stress σ_a in the specimen is calculated from the confining pressure and the pressure applied in the tension force production chamber P_1, the area of the wing of loading piston A_p, the cross-sectional area of sample A_s, and the friction F_f at the contacts, i.e.

$$\sigma_a = \frac{A_p(P_c - P_1) \mp F_f}{A_s} \tag{2}$$

If $P_c \geq P_1$, minus is taken in the sign $\mp$; otherwise, plus is taken. In our design, $A_p = A_s$.

The axial strain ε_1 is either measured by the axial strain gage or calculated from the axial displacement change ΔL recorded by the LVDTs and the initial length of specimen L_0; the lateral (radius) strain is measured either by the lateral strain gage or calculated from the diameter change ΔD of the circumferential ring and the initial specimen diameter D_0, i.e.

$$\varepsilon_1 = \frac{\Delta L}{L_0} \times 100\% \tag{3}$$

$$\varepsilon_3 = \frac{\Delta D}{D_0} \times 100\% \tag{4}$$

3 Material and Method

3.1 Material characterization and sample preparation

The material tested is a type of quartz sandstone drilled from the Fontainebleau town in Southeast of Paris. The fontaintebleau sandstone has been characterized in some previous work[40-44] due to its good homogeneity in calibrating numerical mechanical models. The quartz sandtone tested in this study is constituted of its major mineral quartz, the inter-grain cement and pores (See Fig. 4), which contains much more quartz than the material tested in the aforementioned previous studies. The pore size varies among the quartz grains. The quartz minerals are distributed in the form of polyhedronal grains. These characteristics are different from the fontainebleau tested in the previous studies[40, 43, 44].

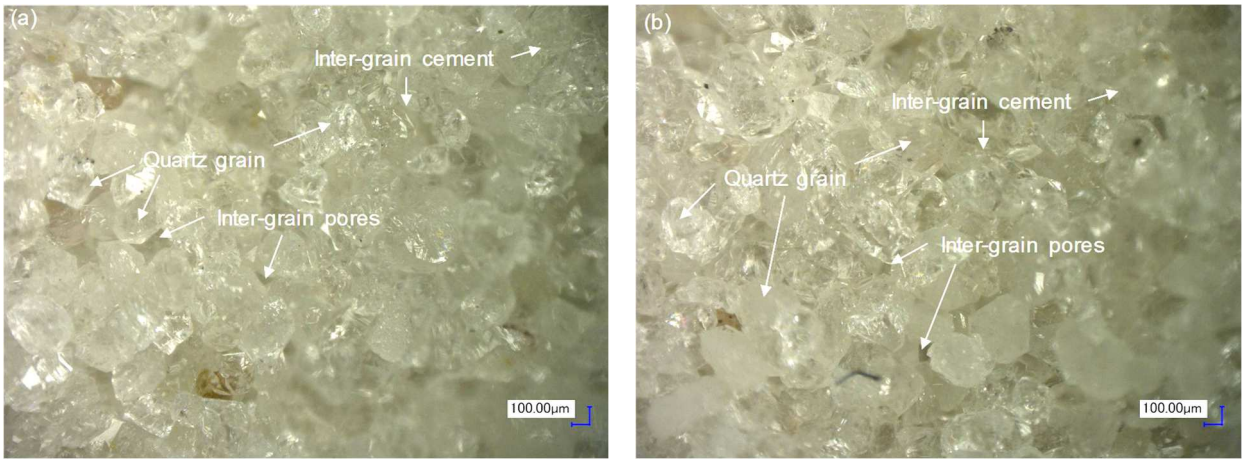

Fig. 4 Optical Microscopy images of tested sandstone

Grains are poorly attached to their neighbors in variety as shown in Fig. 4 (a) and (b). The image in Fig. 4 shows that the serrated grain boundaries are related to authigenic quartz cements, which is similar to a variaty of the sandstone observed in the previous work [42, 43]. The inter-grain cement has a very small amount in contrast to the quartz grain in Fig. 4, which would eventually induce that the physical cohesion of the quartz sandstone is not strong.

The cylindrical specimens used in this study with about 20mm in diameter and 40mm in height were drilled in the laboratory from a cubic block of 500 mm in edge. The drilled specimens were cut and polished on both ends to make the end surface flat and perpendicular to the cylindrical axis. Then, they were kept in an oven that can provide dry air of 30℃ to keep a homogeneous air-dry state in the samples before they were subjected to mechanical tests. The initial diameter and length of the specimens are given in Table 1.

3.2 Experimental program and protocol

We used the developed TDT apparatus to carry out triaxial tension tests on the Fontainebleau quartz sandstone. In order to investigate the effect of confining pressure on the tension behavior of the sandstone, triaxial tension tests under four different confining pressures (0, 2, 6, 12 MPa) were carried out (see Table 1).

In addition, a series of CTC tests under different confining pressures were carried out on the Fontainebleau sandstone to address the relationship between its triaxial tensile and compressive strength. The experimental program is shown in Table 1.

Two repeated experiments were carried out to verify the obtained tensile strength of the developed TDT apparatus under each confining pressure with two specimens. In total, nine different confining pressures

(respectively 0, 2, 4, 6, 10, 16, 20, 30, 40 MPa) were tested for the quartz sandstone in the CTC tests in order to obtain its failure criterion under CTC.

Table 1 : Sample geometry, experimental program and peak stress of all tests

Sample No.	Diameter (mm)	Length (mm)	Test type	P_c (MPa)	Peak axial stress (MPa)	Peak differential stress q (MPa)
T01	19.85	40.25	TDT	0	-1.94	-1.94
T02	19.82	39.85		0	-2.06	-2.06
T03	19.79	39.92		2	-1.79	-3.79
T04	19.86	39.78		2	-1.70	-3.70
T05	19.81	39.81		6	-1.46	-7.46
T06	19.83	39.76		6	-1.40	-7.40
T07	19.84	39.77		12	-1.35	-13.35
T08	19.82	39.81		12	-1.31	-13.31
C01	19.87	39.83	CTC	0	33.67	33.67
C02	19.79	39.84		2	74.34	72.34
C05	19.78	39.88		4	172.76	168.76
C06	19.75	39.81		6	166.55	160.55
C08	19.83	39.86		10	219.46	209.46
C10	19.85	39.83		16	306.69	290.69
C11	19.86	39.85		20	336.28	316.28
C16	19.82	39.86		30	458.71	428.71
C17	19.86	38.79		40	499.17	459.17

The CTC tests were carried out following the protocole of our previous hydro-mechanical tests [45] with our conventional triaxial testing device while neglecting the steps for pore pressure treatments. The TDT tests were carried out with the following protocol to minimize the uncertainty and artifacts in the obtained results. The protocol includes the following steps:

(i) Clean the surface of the specimen supporting base and head successively with distilled water, dry compressed air, pure Arcetone and compressed air, and clean the end surfaces of the sandstone sample with dry compressed air.

(ii) Put a plastic sealing jacket outside the specimen and install the circumferential ring outside the sealing jacket.

(iii) Daub the two end surfaces of the sandstone specimen, and the connnecting surface of the specimen supporting base and head with a very thin layer of the DELO-CA cement.

(iv) Cement the specimen up- and down- end surface respectively with the specimen supporting head and base in the cementation device that can apply a small compression force to allow the homogeneity of the cement at the contacting surface. The cement curing takes more than 48 hours so that the cement strength can grow fully to cement the specimen together with the supporting base and head at both ends. It should be stated that the cementation device controls the centralization of the specimen axis, and the axis of the specimen supporting base and head by setting the specimen and supports on the pre-made fillister.

(v) Install the specimen together with the supporting base and head on the device base with by screwing tight the connecting screw and seal well the sealing jacket after checking the cementation manually with a gentle pulling force.

(vi) Install the LVDTs and the accessories for deformation measurement, and seal the main triaxial chamber by installing the chamber wall and cap, and screwing the pull rods.

(vii) Close the valve between the main triaxial chamber and autocompensated chamber while keep open the valve connecting tension force production chamber, and inject oil into the autocompensated chamber (by the tube 20 in Fig. 2) at a slow rate to allow the loading piston moving downward into the pre-made fillister of the specimen supporting head. Stop the injection once there is a sudden rise in the injected pressure which indicates the piston is pushed on the top of the specimen supporting head.

(viii) Open the valve (in tube 22 in Fig. 2) between the main triaxial chamber and autocompensated chamber, inject oil into the main chamber, and then apply the confining pressure to the prescribed value, e.g. 6.00 MPa, with a hydro-servo pump at a given rate of 0.05 MPa per minute (after closing the valve in tube 20 in Fig. 2) and finally hold the prescribed value.

(viiii) Inject oil into the tension force production chamber (component 16 in Fig. 2) till specimen failure at a constant flow rate of 0.01 ml/min that corresponds to a quasi constant axial strain rate of $10^{-6}/s$ based on the prior essays. During the injection, the specimen experiences firstly an axial extension process and then an

axial direct tension process before direct tension failure.

Throughout the testing process, the values of the pressures, the LVDTs and the circumferential ring are monitored and recorded in the data acquisition device at a given interval of 0.05s. In addition, no pore pressure is applied in the test. Thus, the tests can be thought to be the drained ones since possible small change of pore volume will exert barely effect on the pore pressure change due to the high compressibility of the air prefilled in the specimen pores.

4 Experimental results

4.1 Stress and strain outputs

The axial stress-strain curves of the TDT tests are shown in Fig. 5 (a) to (d) for the confining pressure of respectively 0, 2, 6, 12 MPa. The differential stress versus axial strain curves are shown in Fig. 6 for all the CTC tests. The peak axial stress and peak differential stress of TDT tests and CTC tests are both listed in Table 1. It should be noted that the sign positive for compression and negative for tensile throughout this manuscript for each stress or strain component.

It is indicated in Table 1 that the peak axial stress varies from about 2 MPa to 1.3 MPa when the confining pressure increases from 0 MPa to 12 MPa. The tensile strength under confining pressure is lower than that without confining pressure. There is an estimation error about 30% if one uses the uniaxial tensile strength to represent its tensile strength under P_c=12MPa.

The peak compressive stress however increases from about 33 MPa to 499 MPa when the confining pressure increases from 0 MPa to 40 MPa. For example, the peak tensile stress is about 1/17 of its peak compressive stress when there is no confining pressure. Thus, there is a huge difference between the values of the peak tensile stress and the peak compressive stress of the sandstone under the same confining pressure.

As indicated in Fig. 5, the strain at failure of the sandstone is varying in the triaxial tension tests under different confining pressures. The axial strains at peak axial stress are about 0.17%, 0.25%, 0.26% and 0.35% respectively for the confining pressure of 0, 2, 6 and 12 MPa. Thus, it seems the sandstone can undergo larger axial strains under higher confining pressures in TDT test.

As shown apparently in Fig. 6, the axial strain at peak differential stress also varies importantly in the CTC tests under different confining pressures. The sandstone undergoes about 0.3% axial strain at failure under Pc= 0MPa while can undertake as large as 2.8% axial strain at failure under Pc=40MPa. The higher

confining pressure seems to enlarge the strain of the sandstone prior to failure under CTC.

Therefore, the axial strain at failure in TDT test is much smaller than that in CTC test, which is similar to the observation of peak axial stress of the two types of tests. However, the Fontainebleau sandstone can undergo larger strains under higher confining pressures in both CTC and tension tests.

(a) P_c= 0MPa

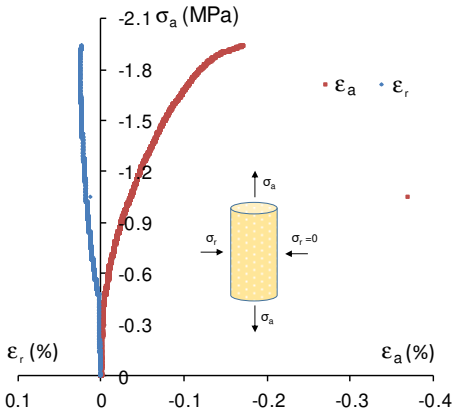

(b) P_c= 2MPa

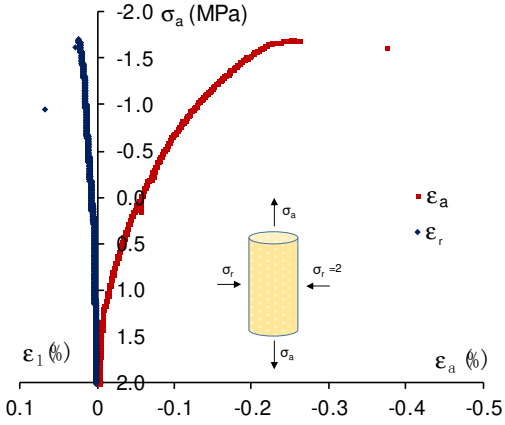

(c) P_c= 6MPa

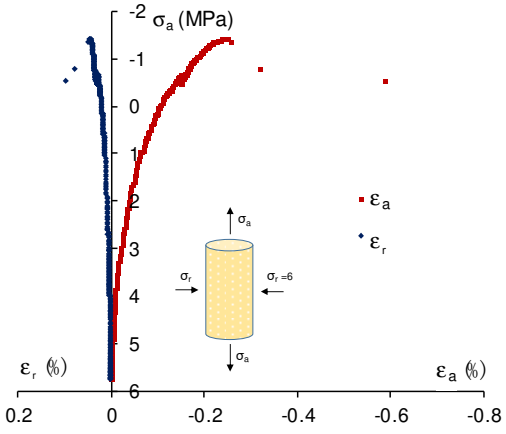

(d) P_c=12MPa

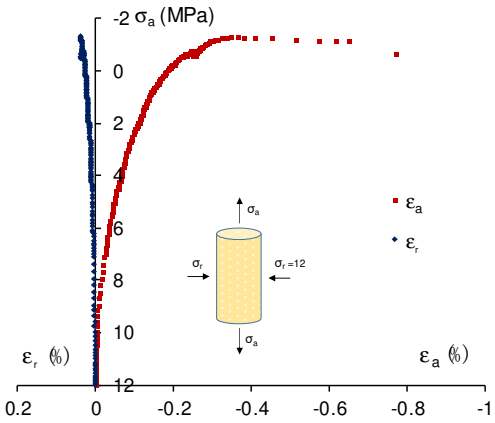

Fig. 5 Axial stress versus strains curves of TDT tests

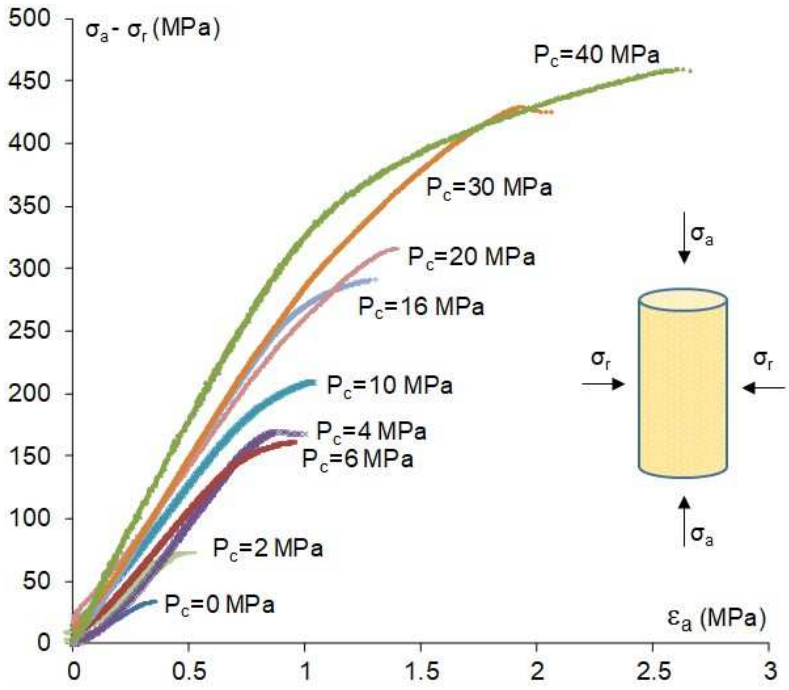

Fig. 6 Differential stress-axial strain curves of all the CTC tests

4.2 Triaxial tensile modulus and Poisson ratio

The tensile modulus (E_t) and Poisson ratio (v) can be calculated from the axial stress versus strain curves in Fig. 5 for each TDT test. The TDT test includes an extension phase and then a tensile phase as shown in Fig. 7. Here we highlight the tensile behavior of the quartz sandstone; thus, we only define the triaxial tensile elastic properties. The extension properties will be investigated in future in tests with extension failure.

In Fig. 7(a), σ_a^{peak} denotes the peak axial stress of the TDT test, and σ_a^{50} denotes the 50% value of peak axial stress. We define E_t and E_t^r the fitted slope of the curve segment where the axial tensile stress increases from 0 to σ_a^{50} on the curve of axial stress respectively versus axial and radius strain as shown in Fig. 7(a). The Poisson ratio v is defined as the ratio of E_t over E_t^r. A similar definition can be also done for the elastic modulus in the CTC tests.

The calculated axial elastic modulus and Poisson's ratio are shown in Fig. 7(b). It is shown that the tensile elastic modulus seems to be decreased by the confining pressure. Its value decreases from 2.0 GPa to 1.2 GPa when the confining pressure increases from 0 to 12 MPa. The Poisson ratio also appears to be influenced by the confining pressure as indicated in Fig. 7(b). The value of Poisson ratio could be affected by the measurement precision of the circumferential ring of the device.

Therefore, the uniaxial tensile elastic modulus of the tested quartz sandstone is about 2.0 GPa and the

confining pressure appears to decrease the tensile elastic modulus. The Poisson's ratio seems also to be affected by the confining pressure in the TDT test.

(a) Definition of tensile elastic modulus

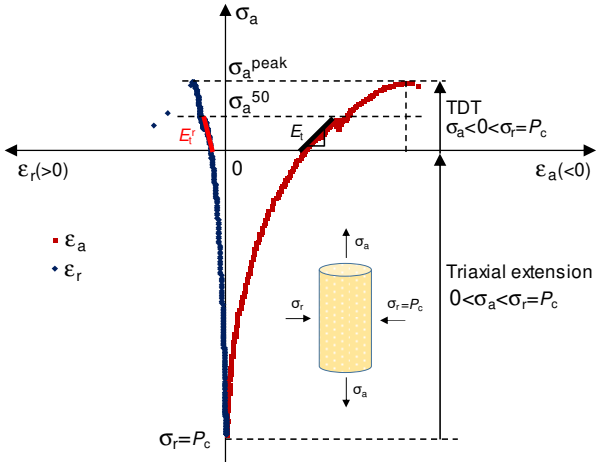

(b) Axial elastic modulus and Poisson's ratio

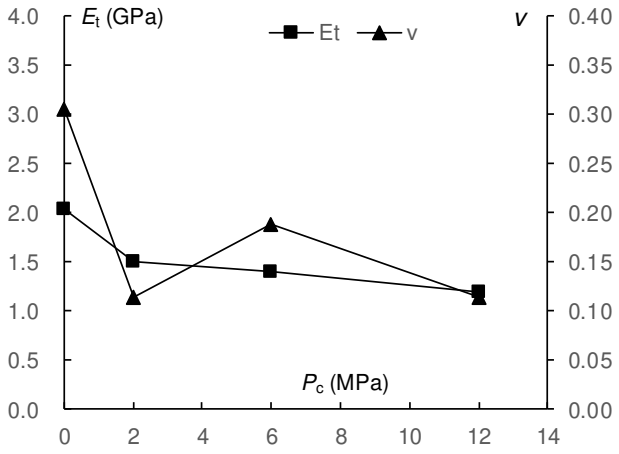

Fig. 7 Definition and the obtained values of tensile elastic parameters from the TDT tests

4.3 Failure mode and post-failure specimen analysis

According to the stress-strain curves shown in Fig. 5 and Fig. 6, it can be concluded that the sandstone exhibits brittle failures in both the TDT and compression tests. Hence, high confining pressure can induce a larger strain of the sandstone prior to failure but contribute barely to its brittle failure.

The post-failure photos of the specimens in tension tests are shown in Fig. 8 to identify the failure surface of the sandstone specimen and to justify its failure mode in TDT tests. The compression failure has been discussed in detail in the literature[44] and thus is not repeated here. It is shown clearly in Fig. 8(a) that the failure surface is formed on a plane for the specimen failed in direct tension without confining pressure. The normal direction of the failure surface is approximately parallel to the axis of the cylindrical specimen. Similar characteristics can be also observed in Fig. 8(b), (c) and (d) for the specimen failed under confining pressure respectively of 2, 6 and 12 MPa. Visually, no apparent difference is exhibited among the failure surface of the specimens failed under different confining pressures. Therefore, the failure surfaces suggest that the quartz sandstone fails with a tensile failure-dominated mode in the TDT tests.

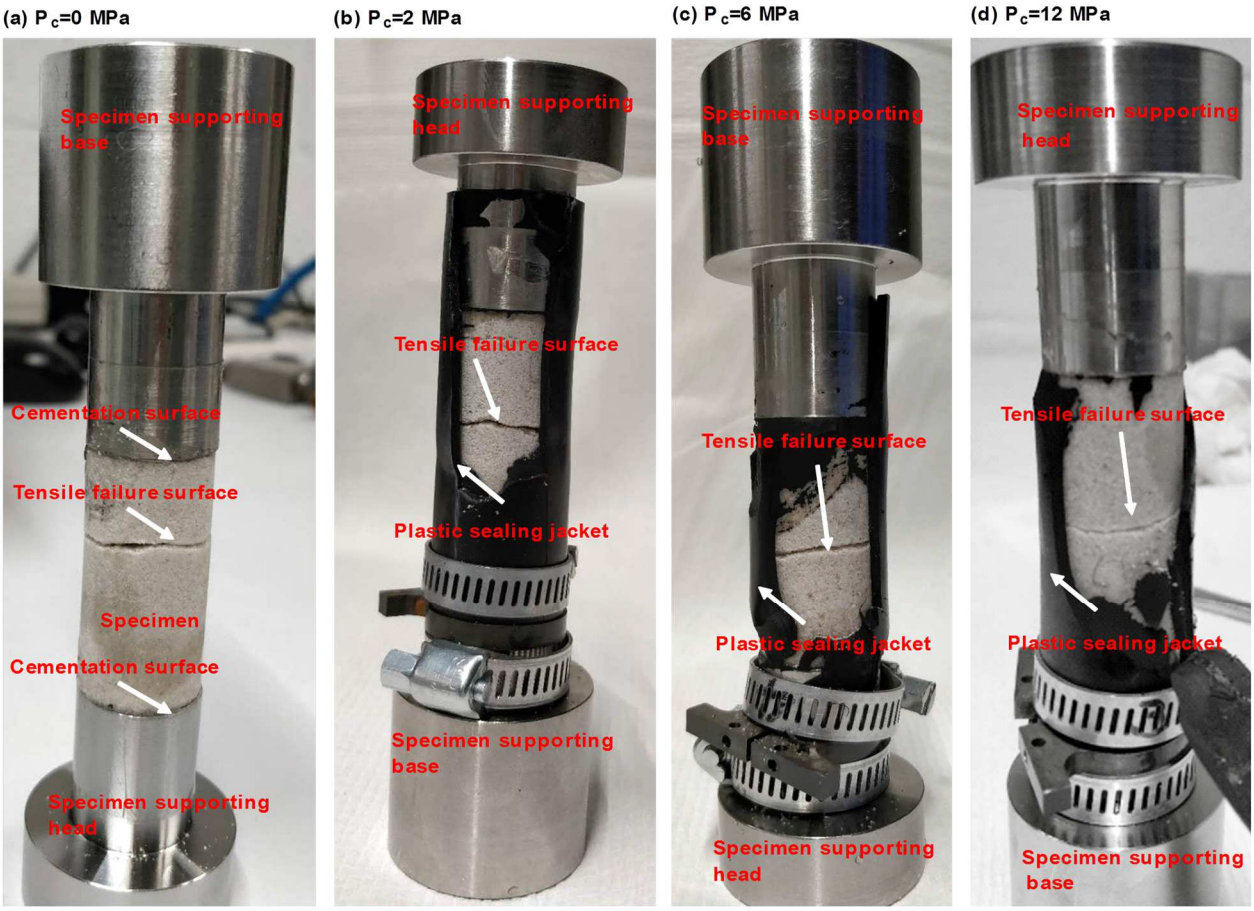

Fig. 8 Post failure photos of representative quartz sandstone specimens after TDT test

To further characterize the failure surface of the specimens after TDT test, we observed the representative sampling points on the failure surface of the specimen failed under different confining pressures by the three-dimensional optical microscopy. The representative images are shown in Fig. 9 which shows that the failure surface is not flat under the microscopy. It should be noted the values of the attitude difference between the peak and the trough on the failure surface would be probably different if different sampling points were observed.

There are apparent peaks and troughs on the failure surfaces. The difference between the peak and the trough varies a lot in Fig. 9(a) to (d), which indicates the difference in roughness of the failure surfaces created under different confining pressures. The maximum difference of the peak and the trough of the four sampling failure surfaces are obtained as 2691.6, 2078.7, 1360.6 and 520.8 micrometers respectively for the confining pressure of 0, 2, 6 and 12 MPa. On this point, one can conclude that the roughness of the failure surface is importantly influenced by the confining pressure. High confining pressure seems to reduce the roughness of the failure surface of the quartz sandstone under TDT failure.

Therefore, the failure of the quartz sandstone in TDT exhibits a typical tensile mode, which is different from the compression-induced shearing failure in the CTC tests. The lateral stress can exert an extra axial extension effect to induce easier tensile failure of the quartz sandstone under TDT.

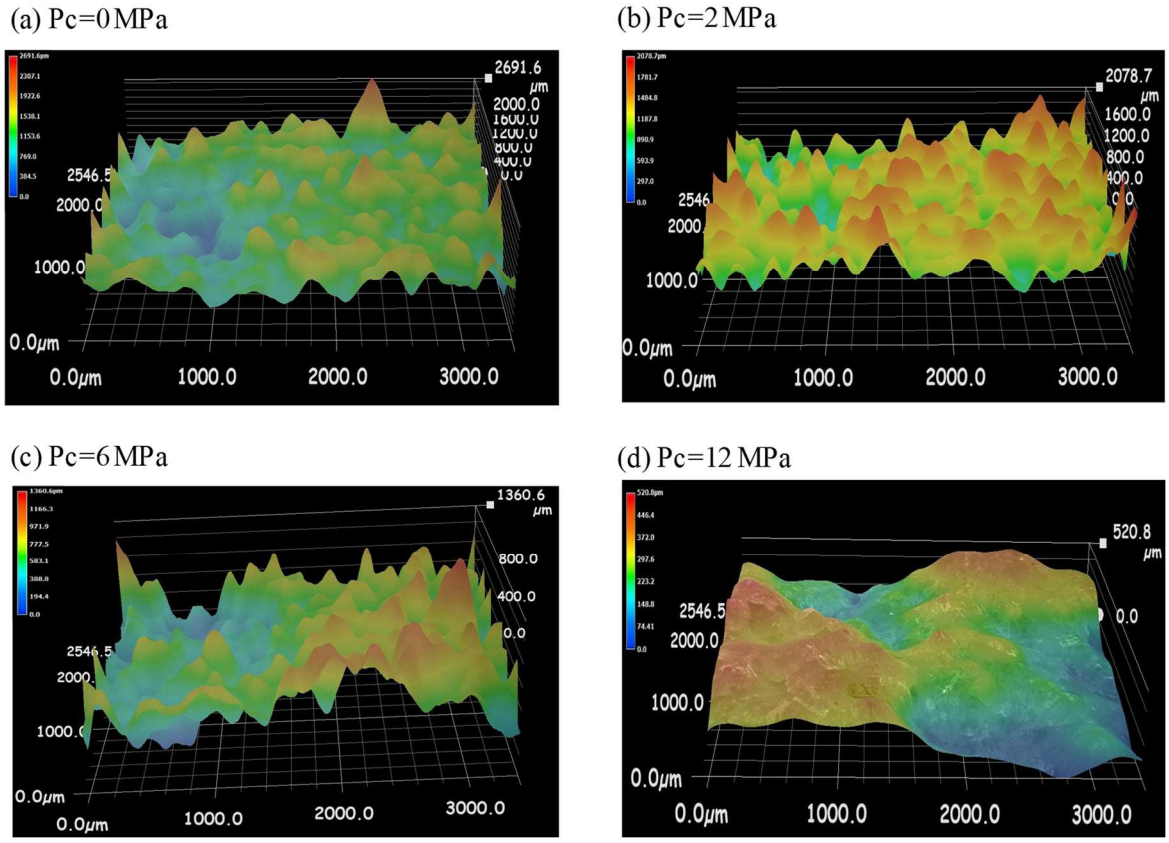

Fig. 9 Three dimensional images of the tensile failure surface under different confining pressure

5 Discussion

5.1 Strength property under CTC and TDT

We define the tensile strength σ_t and the compressive strength σ_c to be the peak axial stress obtained respectively during the triaxial tension and CTC test at a given confining pressure. We obtain the relationship between the tensile/compressive strength and the confining pressure of the quartz sandstone as shown in Fig. 10 according to the data in Table 1.

The Lode's constant μ_σ and Lode angle θ_σ for CTC and TDT test are

$$\begin{cases} \mu_\sigma = 1, \theta_\sigma = 30° & \text{for CTC} \\ \mu_\sigma = -1, \theta_\sigma = -30° & \text{for TDT} \end{cases} \tag{5}$$

The tensile strength of the quartz sandstone is very low compared to its compressive strength as indicated in Table 1 and Fig. 10. The quartz sandstone tensile strength is about 1/17 of its compressive strength if no confining pressure is applied. If the confining pressure is applied, the ratio between the tensile and compressive strength becomes even small. Therefore, the strength of the tested quartz sandstone is importantly influenced by loading path and the Lode's angle.

The compressive strength σ_c of the quartz sandstone (see Fig. 10 (a)) increases with the confining pressure, which is similar to those obtained in the previous studies[43, 44]. The linear Mohr-Coulomb criterion can describe the relationship between the compressive strength and the confining pressure. The obtained cohesion of the Fontainebleau quartz sandstone is about c=20.0 MPa, and the friction angle is φ=55.1°. In the literature[43], the coarse Fontainebleau sandstone has a cohesion c=15.5 MPa and a friction angle φ=41.3°. The comparison of the two values suggest that the Fontainebleau quartz sandstone has a much higher strength than the Fontainebleau sandstone[43] under compression. The difference could probably be induced by the difference in mineral composition and inter-grain cementations of two materials. The tested quartz sandstone is mainly composed of quartz with very thin cement among quartz particles while the coarse sandstone has less quartz in percentage and is cemented by more epoxy among the mineral particles[44].

(a) for CTC

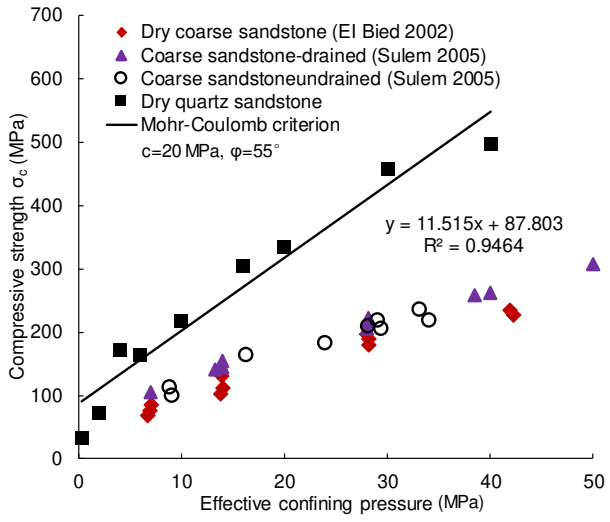

(b) for TDT

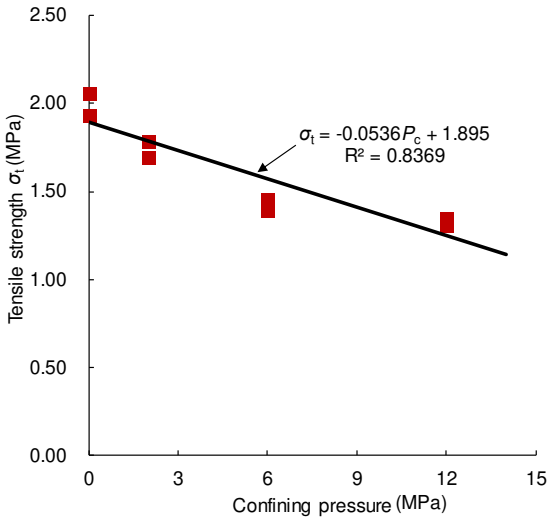

Fig. 10 Strength locus of Fontainebleau quartz sandstone in triaxial test

In contrast, as shown in Fig. 10 (b), the tensile strength of the quartz sandstone decreases with the confining pressure. This decrease feature is similar to that reported by a group of Brazilian tests with axial loads[14]. The tensile strength criterion can be quantified approximately by a linear function, i.e.

$$\sigma_t = \eta P_c + \zeta \tag{6}$$

where η and ζ are material parameters that can be obtained by fitting experimental data. The parameter η quantifies the effect of confining pressure on direct tensile strength; ζ is an estimation of the uniaxial tensile strength. According to the triaxial tension test data in Table 1, one can obtain $\eta = -0.0536$, $\zeta = 1.895$ as shown in Fig. 10 (b).

One can see that the confining pressure plays an important role in increasing the compressive strength of the quartz sandstone from the parameter $\eta = 11.515$ of the strength criterion for compression (see Fig.9(a)). However, the contribution of the confining pressure in triaxial tension is limited although it induces a decrease of the tensile strength with parameter $\eta = -0.0536$. Thus, stress state can affect importantly the tensile failure of rocks.

The triaxial tensile strength decrease could be partially contributed by the effect of Poisson's ratio. When a lateral stress $\sigma_3>0$ is applied, it can induce tensile strains in the directions of sample axis due to the Poisson's ratio effect. Hence it requires a lower tensile stress to pull the specimen in its axial direction. This effect is similar to that in the triaxial extension test of rocks[14]. Therefore, the TDT strength of the quartz sandstone is dominated by its uniaxial tensile strength that is attributed to the cementation forces among the mineral particles. Confining pressure can induces a decrease of the TDT strength attributed to the Poisson's ratio effect.

5.2 Failure criterion from compression to tension

It is difficult to correlate the tensile strength to the compressive strength from the equations obtained in Fig. 10. We could conduct a further failure stress analysis to derive a failure criterion for possible constitutive modeling based on the data obtained. For convenience, we define the mean stress σ_m and differential stress q respectively as

$$\sigma_m = (\sigma_a + 2\sigma_r)/3, \quad q = \sigma_a - \sigma_r \tag{7}$$

where, σ_a and σ_r are respectively the axial stress and radius stress.

We can thus recollect the mean stress σ_m and differential stress q obtained from both TDT and CTC tests as given in Table 1 and shown in Fig. 11. It is indicated that the tensile strength is decreased while the compression strength is increased by the confining pressure in triaxial tests. To describe the stress relationships, one can use the linear criterion

$$q = \kappa\sigma_m + \psi \tag{8}$$

where the parameters κ and ψ are material constants that can be obtained from experimental data.

As indicated in Fig. 11(a), the linear criterion in Eq.(8) with the parameters $\kappa = 2.4152, \psi = 9.868$ and $\kappa = -1.382, \psi = -2.7692$ could the best fitting of the relationship between the mean stress and differential stress obtained respectively from the CTC and TDT testing data of the quartz sandstone. The digits in the grey brackets in Fig. 11(a) are the absolute relative errors in percent of the experimental data estimated by the linear criterion with the given parameters. The envelopes for CTC and TDT in Fig.10 indicate that the failure criterion of the quartz sandstone is also influenced by the Lode's angle.

The slope value of the linear criteria for the CTC tests (2.4152) is much greater than that of the TDT tests (1.382). The value of the slope is a quantification of the "friction effect" contributed by the P_c. Thus, the P_c-induced friction has a much significant effect on the strength of the quartz sandstone under CTC than under TDT. It is also probably the reason why, as indicated by the post-failure photos in Fig. 8, the failure mode and mechanisms of the quartz sandstone under TDT are different from those under CTC.

The envelope of linear criterion of the CTC test and TDT test intersects the σ_m axis respectively at the point V_{0C} and V_{0T}. The results show that the envelope is not symmetric to the σ_m axis from compression to tension, which indicates that the strength of the tested quartz sandstone is sensitive to the Lode's angle. The point V_{0T} or V_{0C} denotes the stress state that the material fails at an isostatic tension stress[46, 47] with q=0. Theoretically, the point V_{0T} or V_{0C} should be coincided to be one vertex at the σ_m axis where the envelops of the CTC and TDT test intersect. As shown in Fig. 11(b), there is a deviation between the point V_{0C} and V_{0T} for the linear criterion in Eq. (8) for the tested sandstone. If the point V_{0C} is the vertex with the point V_{0T} (see Fig. 11(b)), the criterion for compression should be nonlinear. Therefore, the shape of the failure envelope of the tested sandstone from compression (θ_σ=30°) to tension (θ_σ=-30) is more complicated than the linear one.

The non-symmetricity and shape difference for tension and compression of the tested quartz sandstone are different from those of the Red Wildmoor sandstone[48]. The envelope of the Red Wildmoor sandstone is symmetric to the σ_m axis from compression to extension[47, 48], indicating that its strength is not sensitive to the Lode' angle. The difference indicates that the strength of the two types of sandstone have different sensitivity to the Lode's angle.

Therefore, the non-symmetricity of the strength envelope of the quartz sandstone indicates that estimation of its triaxial tensile strength from the CTC test can induce an important overestimation. Triaxial tensile strength of the high-frictional geomaterials such as the quartz sandstone should be determined by the

TDT tests. The failure criterion for constitutive modeling of the quartz sandstone from compression to tension is suggested to be non-symmetric with respect to the mean stress axis.

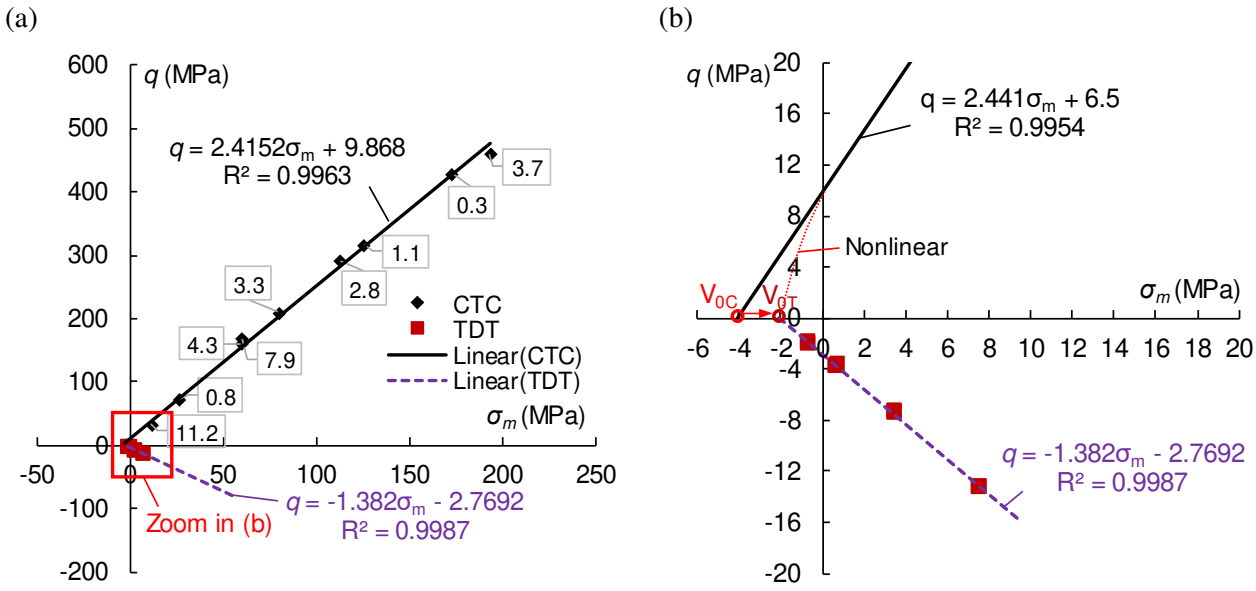

Fig. 11 Stress analysis in $q-\sigma_m$ plane for TDT and CTC test.

6 Concluding remarks

Based on the results presented above, the following concluding remarks can be drawn:

(1) The TDT test on rocks with the developed apparatus modified from the conventional triaxial cell is feasible with the cementing method although preparation of specimen is a little complicated. Boundary conditions are critical in the TDT test. The performance of the cementing is the main limited issue for carrying out successful tests under high confining pressures since the confining stress can exert a lateral shear force to the specimen at the cementing surface.

(2) The tensile strength of the quartz sandstone is very low compared to the compressive one. The uniaxial tensile strength is no more than 1/17 of its uniaxial compressive strength. The ratio of triaxial tensile strength to triaxial compressive strength is even smaller when the confining pressure is high. The direct tensile strength of quartz sandstone could be dominated by the cementation among its mineral particles.

(3) Confining pressure increases and dominates the triaxial compressive strength of quartz sandstone under CTC. However, it decreases its triaxial tensile strength and elastic modulus under the TDT. The confining pressure contributes to the normal stress for friction on the compression-induced shear surface in compression tests while it accelerates the axial tension of the specimen under direct tension, e.g. with the

Poisson ratio effect.

(4) Tensile failure planes of the quartz sandstone under TDT tests are generally perpendicular to the axis of the specimen, i.e. parallel to the direction of tensile stress. The confining pressure has very limited effects on the failure surface inclination of the quartz sandstone under the TDT tests although the surface roughness seems to be influenced by the confining pressure.

(5) Triaxial tensile strength of the high-frictional geomaterials such as the quartz sandstone should be determined by the TDT tests since the estimation of its triaxial tensile strength from the CTC test can induce an important overestimation. The failure criterion for constitutive modeling of the quartz sandstone from compression to tension is suggested to be non-symmetric with respect to the mean stress axis.

Nevertheless, the performance of the developed TDT device is limited by the cementing performance and the quality in cementation of the specimen. Artifacts in cementing specimen with the supporting base and head would induce bad centralization of the tension in test, and finally induce odd failures and experimental data. In addition, the cement and the specimen support base and head must be also well designed to be able to fit with different rocks in future work. Comparison on triaxial extension, CTC and TDT tests will be investigated in future.

Acknowledgements

The authors are grateful to Mr. Jean Secq for his help in design of the TDT device. The authors also thank Dr. Nicolas Gay and Professor Fréderic Skoczylas for their help in the specimen study with the optical microscopy. Financial support to Zaobao Liu from the Fundamental Research Funds for Central Universities of China (N180105031), the Young Talent Program of Liaoning Province (XLYC1807094), and the Research and Development Program of Anhui Province (no.1804b06020361) and Sichuan Province(no.2019YFG0047) are acknowledged.

Reference

1. Diederichs MS, Kaiser PK. Tensile strength and abutment relaxation as failure control mechanisms in underground excavations. *Int J Rock Mech Min Sci.* 1999;36(1): 69-96.

2. Fuenkajorn K, Klanphumeesri S. Direct Tension Tests of Intact Rocks Using Compression-to-Tension Load Converter. *Research and Development Journal.* 2010;21(2): 51-57.

3. Akazawa T. New test method for evaluating internal stress due to compression of concrete: the splitting tension test. *J Japan Soc Civil Eng.* 1943;29: 777-787.

4. Carneiro F. A new method to determine the tensile strength of concrete. *the 5th meeting of the Brazilian Association for Technical Rules.* 3. San Paulo; 1943:126-129.

5. ISRM. Suggested methods for determining tensile strength of rock materials. *International Journal of Rock Mechanics and Mining Sciences & Geomechanics Abstracts.* 15. 1978:99-103.

6. Li D, Wong LNY. The Brazilian Disc Test for Rock Mechanics Applications: Review and New Insights. *Rock Mech Rock Eng.* 2013;46(2): 269-287.

7. Hudson JA. Tensile strength and the ring test. *Int J Rock Mech Min Sci & Geomech Abstr.* 1969;6(1): 91-97.

8. Pandey P, Singh DP. Deformation of a rock in different tensile tests. *Eng Geol.* 1986;22(3): 281-292.

9. Newman DA, Bennett DG. The effect of specimen size and stress rate for the Brazilian test—A statistical analysis. *Rock Mech Rock Eng.* 1990;23(2): 123-134.

10. Barla G, Innaurato N. Indirect tensile testing of anisotropic rocks. *Rock Mechanics.* 1973;5(4): 215-230.

11. Xu S, De Freitas MH, Clarke BA. The Measurement of Tensile Strength of Rock. *ISRM International Symposium.* Madrid, Spain: International Society for Rock Mechanics and Rock Engineering; 1988:8.

12. Coviello A, Lagioia R, Nova R. On the Measurement of the Tensile Strength of Soft Rocks. *Rock Mech Rock Eng.* 2005;38(4): 251-273.

13. Hiramatsu Y, Oka Y. Determination of the tensile strength of rock by a compression test of an irregular test piece. *Int J Rock Mech Min Sci & Geomech Abstr.* 1966;3(2): 89-90.

14. Phueakphum D, Fuenkajorn K, Walsri C. Effects of intermediate principal stress on tensile strength of rocks. *Int J Fract.* 2013;181(2): 163-175.

15. Luong MP. Direct Tensile And Direct Shear Strengths Of Fontainebleau Sandstone. *The 29th U.S. Symposium on Rock Mechanics (USRMS).* Minneapolis, Minnesota: American Rock Mechanics Association; 1988:12.

16. Nova R, Zaninetti A. An investigation into the tensile behaviour of a schistose rock. *Int J Rock Mech Min Sci & Geomech Abstr.* 1990;27(4): 231-242.

17. Jyh Jong L, Yang M-T, Hsieh H-Y. Direct tensile behavior of a transversely isotropic rock. *Int J Rock Mech Min Sci.* 1997;34(5): 837-849.

18. Fuenkajorn K, Klanphumeesri S. Determination of Direct Tensile Strength And Stiffness of Intact Rocks.

ISRM International Symposium - EUROCK 2010. Lausanne, Switzerland: International Society for Rock Mechanics and Rock Engineering; 2010:4.

19. Jensen SS. Experimental Study of Direct Tensile Strength in Sedimentary Rocks. *Department of Petroleum Engineering and Applied Geophysics.* Master. Norwegian University of Science and Technology; 2016:111.

20. Zhang Q, Duan K, Xiang W, Yuan S, Jiao Y. Direct Tensile Test on Brittle Rocks with the Newly Developed Centering Apparatus. 2018.

21. Wu C, Chen X, Hong Y, Xu R, Yu D. Experimental Investigation of the Tensile Behavior of Rock with Fully Grouted Bolts by the Direct Tensile Test. *Rock Mech Rock Eng.* 2018;51(1): 351-357.

22. Shang J, West LJ, Hencher SR, Zhao Z. Tensile strength of large-scale incipient rock joints: a laboratory investigation. *Acta Geotech.* 2018;13(4): 869-886.

23. Hoek E. Fracture of anisotropic rock. *J S Afr Inst Min Metall.* 1964;64(10): 501-518.

24. Brace W. Brittle fracture of rocks. In: Judd W, ed. *the International Conference on State of Stress in the Earth's Crust.* New York: Elsevier; 1964:111-174.

25. Gorski B. Tensile testing apparatus. United States; 1993.

26. Vutukuri V, Lama R, SS S. *Handbook on mechanical properties of rocks*. Ohio, USA: Trans Tech Publications; 1974.

27. Kahraman S, Fener M, Kozman E. Predicting the compressive and tensile strength of rocks from indentation hardness index. *J South Afr Inst Min Metall.* 2012;112: 331-339.

28. Perras MA, Diederichs MS. A Review of the Tensile Strength of Rock: Concepts and Testing. *Geotech Geol Eng*. 2014;32(2): 525-546.

29. Obert L, Windes S, Duvall W. *Standardized tests for determining the physical properties of mine rock*: U.S.B.M.R.I. 3891; 1946.

30. Fairhurst C. Laboratory measurement of some physical properties of rock. *4th Symposium on Rock Mechanics.* University Park Penn.; 1961:105-118.

31. Hawkers I, Mellor M. Uniaxial testing in rock mechanics laboratories. *Eng Geol.* 1970;4: 177-285.

32. Brace W. Brittle fracture of rocks. *International Conference on State of Stress in the Earth's Crust.* Santa Monica, California; 1963:110-174.

33. Liu Z, Shao J. Strength behavior, creep failure and gas permeability change in a tight marble under triaxial compression. *Rock Mech Rock Eng.* 2017;50(3): 529-541.

34. Liu ZB, Xie SY, Shao JF, Conil N. Multi-step triaxial compressive creep behaviour and induced gas permeability change of clay-rich rock. *Géotechnique.* 2018;68(4): 281-289.

35. Han B, Xie SY, Shao JF. Experimental Investigation on Mechanical Behavior and Permeability Evolution of a Porous Limestone Under Compression. *Rock Mech Rock Eng.* 2016;49(9): 3425-3435.

36. Liu Z, Shao J, Xie S, Conil N, Zha W. Effects of relative humidity and mineral compositions on creep deformation and failure of a claystone under compression. *Int J Rock Mech Min Sci.* 2018;103: 68-76.

37. Han B, Shen WQ, Xie SY, Shao JF. Influence of pore pressure on plastic deformation and strength of limestone under compressive stress. *Acta Geotech.* 2018.

38. Liu Z, Shao J, Xie S, Conil N, Talandier J. Mechanical Behavior of Claystone in Lateral Decompression Test and Thermal Effect. *Rock Mech Rock Eng.* 2018.

39. Liu ZB, Shao JF, Hu DW, Xie SY. Gas Permeability Evolution with Deformation and Cracking Process in a White Marble Under Compression. *Transp Porous Media.* 2016;111(2): 441-455.

40. Saadi FA, Wolf K-H, Kruijsdijk Cv. Characterization of Fontainebleau Sandstone: Quartz Overgrowth and its Impact on Pore-Throat Framework. *J Pet Environ Biotechnol.* 2017;7: 328.

41. Chen M, Li M, Wang Y, Zhao J-Z, Xiao W-L. The permeability of fontainebleau sandstone to gases and liquids. *Pet Sci Technol.* 2016;34(9): 845-852.

42. Song I, Renner J. Hydromechanical properties of Fontainebleau sandstone: Experimental determination and micromechanical modeling. *J Geophys Res.* 2008;113(B09211): 1-16.

43. Sulem J, Ouffroukh H. Hydromechanical Behaviour of Fontainebleau Sandstone. *Rock Mech Rock Eng.* 2005;39(3): 185-213.

44. El Bied A, Sulem J, Martineau F. Microstructure of shear zones in Fontainebleau sandstone. *Int J Rock Mech Min Sci.* 2002;39(7): 917-932.

45. Liu ZB, Shao JF, Liu TG, Xie SY, Conil N. Gas permeability evolution mechanism during creep of a low permeable claystone. *Appl Clay Sci.* 2016;129: 47-53.

46. Meyer JP, Labuz JF. Linear failure criteria with three principal stresses. *Int J Rock Mech Min Sci.* 2013;60: 180-187.

47. Labuz JF, Zeng F, Makhnenko R, Li Y. Brittle failure of rock: A review and general linear criterion. *J Struct Geol.* 2018;112: 7-28.

48. Papamichos E, Tronvoll J, Vardoulakis I, et al. Constitutive testing of Red Wildmoor sandstone. *Mechanics of Cohesive-frictional Materials.* 2000;5(1): 1-40.